iScience

CellPress
OPEN ACCESS

Article

Lichens Bite the Dust – A Bioweathering Scenario in the Atacama Desert

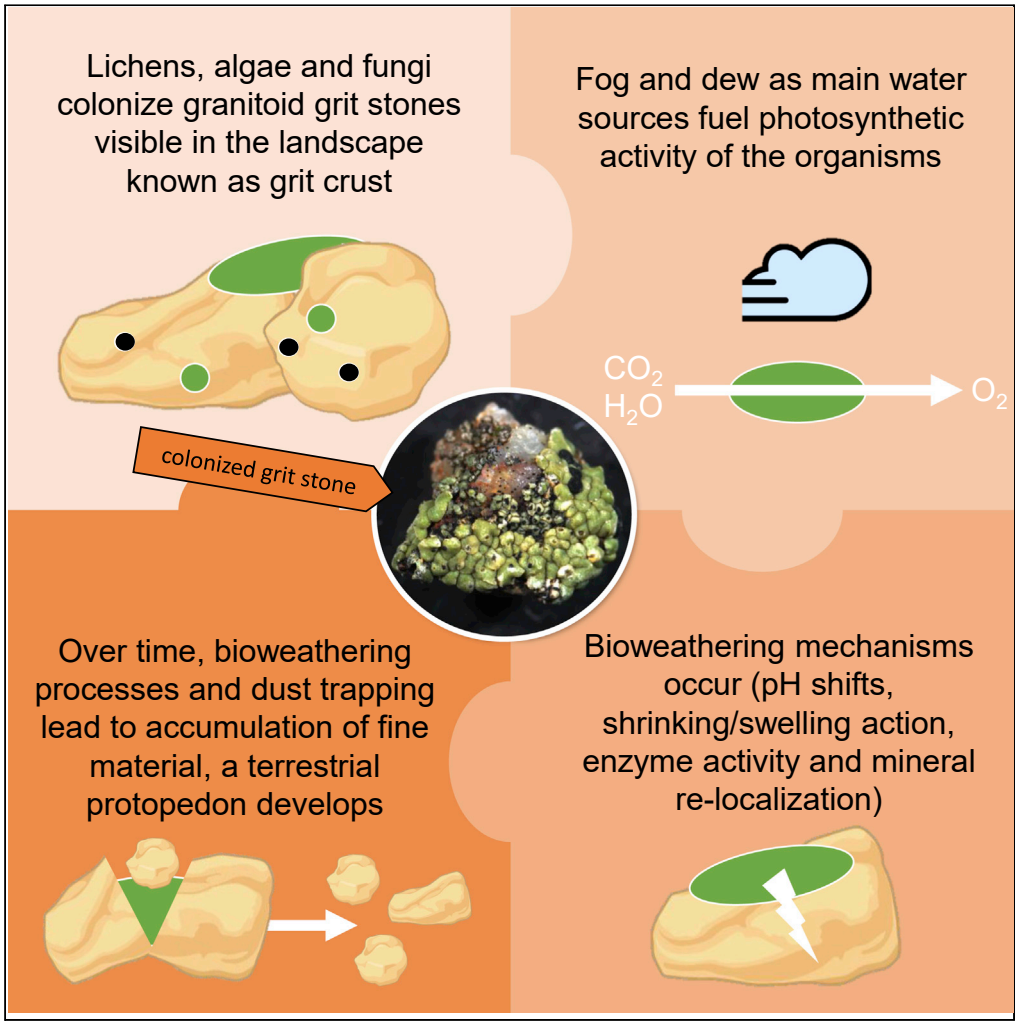

Patrick Jung, Karen Baumann, Dina Emrich, ..., Marcus Frank, Burkhard Büdel, Peter Leinweber

patrick_jung90@web.de

HIGHLIGHTS

A microbial community in the Atacama Desert mediates diverse bioweathering processes

Lichens, algae, and heterotrophic microbes lead to the deterioration of small stones

Detection of swelling actions, shifts in pH, enzyme activity, and mineral transports

Formation of a terrestrial protopedon as initial stage of soil on landscape scale

Jung et al., iScience *23*, 101647
November 20, 2020
https://doi.org/10.1016/j.isci.2020.101647

iScience

CellPress
OPEN ACCESS

Article

Lichens Bite the Dust – A Bioweathering Scenario in the Atacama Desert

Patrick Jung,[1,9,*] Karen Baumann,[2] Dina Emrich,[3] Armin Springer,[4,5] Vincent J.M.N.L. Felde,[6] Stefan Dultz,[7] Christel Baum,[2] Marcus Frank,[4,5] Burkhard Büdel,[8] and Peter Leinweber[2]

SUMMARY

Bioweathering mediated by microorganisms plays a significant role in biogeochemical cycles on global scales over geological timescales. Single processes induced by specific taxa have been described but could rarely be demonstrated for complex communities that dominate whole landscapes. The recently discovered *grit crust* of the coastal Atacama Desert, which is a transitional community between a cryptogamic ground cover and a rock-bound lithic assemblage, offers the unique chance to elucidate various bioweathering processes that occur simultaneously. Here, we present a bioweathering scenario of this biocenosis including processes such as penetration of the lithomatrix, microbial responses to wet-dry cycles, alkalinolysis, enzyme activity, and mineral re-localization. Frequently occurring fog, for example, led to a volume increase of microorganisms and the lithomatrix. This, together with pH shifts and dust accumulation, consequently results in biophysical breakdown and the formation of a *terrestrial protopedon*, an initial stage of pedogenesis fueled by the *grit crust*.

INTRODUCTION

Early development of terrestrial ecosystems often includes interactions between cryptogamic lithobiontic communities (cyanobacteria, green algae, lichens, and fungi together with other heterotrophic organisms), the lithomatrix of rocks and the given climatic conditions (Mergelov et al., 2018; Mitchell et al., 2019). Since the occurrence of life on Earth, the interplay between the biotic and abiotic world is amongst the most ancient processes shaping the earth's surface. For example, the symbiotic interaction between algae and fungi in lichens probably dates back to the Precambrian 400 million years ago (Taylor et al., 1995) although there is evidence for a later origin of modern lichens dating back 320 million years (Lumbsch and Rikkinen, 2017; Nelsen et al., 2020). However, the terrestrial organic carbon (C_{org}) pool of early soils has been fueled to a large extend by the biological activity of cyanobacteria, later supported by algae and fungi until land plants appeared roughly 300 million years ago.

Nowadays, lithobiontic communities are still well known from arid environments such as the Atacama Desert (Azúa-Bustos et al., 2011), where not only external surfaces of hard rocks but also cracks and fissures may be conquered by microorganisms using bioreceptive characteristics of the internal rock structure (Wierzchos et al., 2015). In this region, fog and dew are the main water sources for photosynthetic activity (e.g. Lehnert et al., 2018). Consequently, the alteration and transformation of the lithomatrix by metabolism and bioweathering processes of phototrophs can be expected (Weber et al., 2011). This was described for extreme habitats such as Antarctica or ancient Mayan buildings (Ortega-Morales et al., 2016) and similar interactions are very likely to occur in the Atacama Desert, but reports are still missing. Single processes of biogeophysical and biogeochemical weathering by (cyano-)bacteria, green algae, lichens, and fungi are well studied (reviewed in Salvadori and Municchia, 2016; Chen et al., 2000). This includes, e.g., the biological transformation of clay minerals, e.g. by K depletion of interlayers of mica/illite and oxidation of structural Fe(II) of less weathering resistant silicates such as biotite as well as the dissolution of phosphate salts such as apatite (Smith, 1978; Wierzchos and Ascaso, 1998; Chen et al., 2000). Many studies investigated the weathering of quartz, one of the most common minerals which is an oxide where the atoms are linked in a framework of SiO_4 that makes quartz one of the most stable minerals in terms of weathering. Various microorganisms were found to mediate biochemical weathering processes of rock-forming minerals such as the excretion of pH shifting substances that interfere with the lithomatrix (acidolysis or alkalinolysis), the production of chelating compounds such as siderophores (complexolysis; Daghino et al., 2010) or the

[1]Applied Logistics and Polymer Sciences, University of Applied Sciences Kaiserslautern, Carl-Schurz-Straße 10-16, 66953 Pirmasens, Germany

[2]Faculty of Agricultural and Environmental Science, Soil Science, University of Rostock, Justus-von-Liebig-Weg 6, 18051 Rostock, Germany

[3]University of Freiburg, Faculty of Environment and Natural Resources, Chair of Applied Vegetation Ecology, Tennenbacher Str. 4, 79106 Freiburg, Germany

[4]Medical Biology and Electron Microscopy Centre, University Medicine Rostock, Strempelstraße 14, 18057 Rostock, Germany

[5]Department Life, Light and Matter, University of Rostock, 18051 Rostock, Germany

[6]Department of Soil Science, Faculty of Organic Agricultural Sciences, University of Kassel, Nordbahnhofstr. 1a, 37213 Witzenhausen, Germany

[7]Institute of Soil Science, Leibniz Universität Hannover, Herrenhäuser Str. 2, 30419 Hannover, Germany

[8]Plant Ecology and Systematics, University of Kaiserslautern, Erwin-Schrödinger-Straße, 67663 Kaiserslautern, Germany

[9]Lead Contact

*Correspondence: patrick_jung90@web.de

https://doi.org/10.1016/j.isci.2020.101647

manipulation of the redox potential via extracellular enzymes (Włodarczyk et al., 2016). Although phototrophs are a focal point of interest for bioweathering processes more and more studies are showing a hidden potential in heterotrophic microorganisms such as basidiomycete fungi (Kirtzel et al., 2020) or bacteria (Matlakowska et al., 2012). However, so far, no study has shown bioweathering activity as the sum of these complex biochemical and biophysical weathering factors during the development of terrestrial ecosystems at the landscape scale, but rather single processes have been documented (e.g. Souza-Egipsy et al., 2004; Büdel et al., 2004).

Contrary to lithobiontic communities which colonize rock surfaces, biocrusts establish on and between unconsolidated inorganic and organic soil compounds. This means that the biocrust organisms grow at the surface of sediment and/or soil or within the upper few mm of the upper soil horizon, rather than directly on the more or less weathered parent rock (Belnap, 2003; Garcia-Pichel et al., 2016). However, investigations on weathering mechanisms and rates mediated by biocrust organisms are still in their infancy. This may be due to a greater predisposition of the lithic habitat to weathering and erosional processes, whereas the soil habitat is already a first result of these processes (Garcia-Pichel et al., 2016). Estimations on weathering rates are not only hindered due to erosional processes but also in cases where the original situation before biocrust formation cannot be reconstructed (a prerequisite for calculation of mass balances) due to the presence of different shares of parent rock materials, e.g. from Aeolian dust inputs from different petrological regions (local sources versus those from long-distance transport). One of the few described processes in the context of biocrust-mediated weathering is the leaching and re-localization of elements mobilized by biogenic processes in deeper soil horizons (Beraldi-Campesi et al., 2009) as well as the accumulation of organic matter, which triggers further pedogenetic processes such as the formation of organo-mineral associations (Dümig et al., 2014). Due to the fact that these are permanent processes in biocrusts, Beraldi-Campesi et al. (2009) speculated that allochthonous (Aeolian dust) inputs compensate for elemental loss in the upper soil mm to maintain the nutrition of biocrusts in the long run. Some rock outcrops can be highly resistant against biochemical weathering due to its coarse mineral grain size, low specific surface area, and the presence of less vulnerable minerals to (bio)chemical weathering such as quartz, alkali feldspars and muscovite in granitic rocks. If this is the case fine-sized deposited Aeolian dust particles containing high shares of layer silicates and also organic compounds can be a major phase for element mining and energy recovery by biocrust organisms.

Recently, a unique transitional community between lithobiontic and biocrust biocenoses, termed *grit crust*, growing around and inside granitoid grit stones of about 6 mm in size (locally called *maicillo*) that are paving the ground in broad areas of the coastal Atacama Desert, was described (Jung et al., 2020). The vivid colonization of the grits by mainly lichens causes a blackish pattern of several square meter large patches on the ground that can be seen across the landscape (hereafter called *black grit*) right beside less colonized grits forming patches that appear whitish (hereafter called *white crust*). The reasons for the scattered presence of the biocenosis in the landscape is still not clarified but seems to be more complex than the simple relation between topography, fog water deposition, and colonization rate (Jung et al., 2020). So far, this biocenosis has been detected to cover locally between 20 and 80% of the 350 km^2 National Park Pan de Azúcar, highlighting its significance in terms of ecosystem services such as nutrient acquisition, water retention or erosion prevention (Jung et al., 2020).

The tight relation between the organisms and the lithomatrix of the grits enabled us to describe a bioweathering scenario mediated by lichens, cyanobacteria, green algae, and fungi that potentially leads to pedogenesis on landscape scales. We hypothesized that complex and various interactions between the *grit crust* organisms and deposited dust, the soil compounds and grit interfaces lead to a physical breakdown of the latter and an accumulation of fine soil particles. For these reasons, an interdisciplinary approach consisting of soil analyses such as mineral composition, dust composition, bioweathering assays such as long-term and short-term pH shifts induced by green algal lichen photobionts, enzyme activity and the shrinking-swelling action of colonized grit stones induced by water was applied. In particular we A) tested to which extend swelling and shrinking of the organisms induced by frequently occurring fog can lead to the physical breakdown of the grit stones, B) tested whether pH shifts caused by the organisms can in turn promote etching of substrate particles and C) characterized the texture and elemental content of the accumulated material which contributes to pedogenesis.

RESULTS

Based on field observations in the National Park Pan de Aúzcar that is situated in the coastal range of the Atacama Desert we found evidence which led to the following bioweathering chronosequence presented

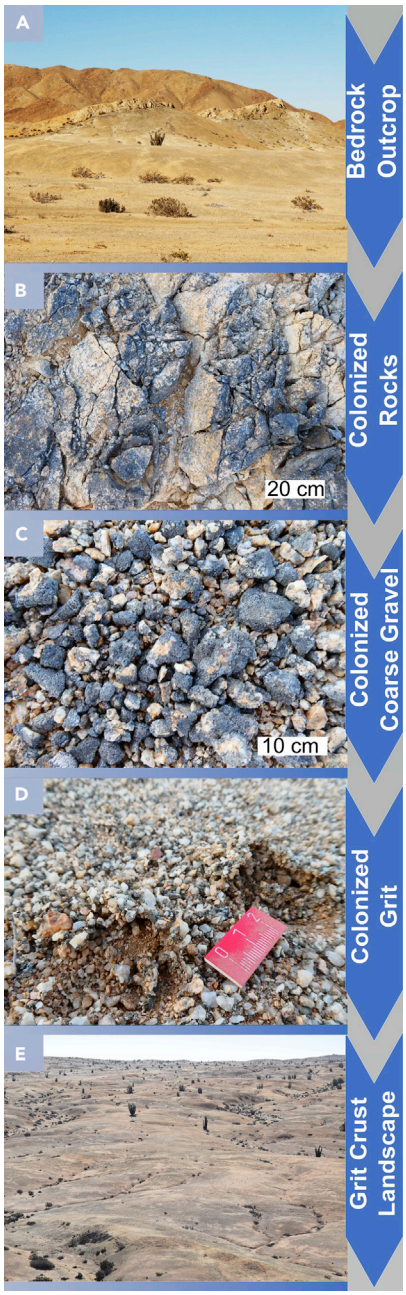

Figure 1. Chronosequence of Bioweathering in the Landscape of the National Park Pan de Azúcar, Atacama Desert

(A) Bedrock outcrop made of granitoid material. (B) Colonized rocks in close vicinity of the bedrock outcrop. Scale bar indicates 20 cm. (C) Colonized coarse gravels in close vicinity of the rocks. Scale bar indicates 10 cm. (D) Grit stones concatenated by organisms. (E) Colonized grit causing blackish patterns in the landscape.

in Figure 1. This sequence depicts the idea of microorganisms such as lichens, algae, fungi, and other heterotrophic organisms colonizing boulders of parent rock in the landscape (Figures 1A and 1B). Subsequently the interplay between abiotic and biotic weathering processes led to the deterioration of the rocks into smaller fragments that were also colonized till the current snapshot in time resulting in the 'grits' (Figure 1C). The grits have a size of roughly 6 mm and cover large areas at least in the National Park Pan de Azúcar (Jung et al., 2020). They appear as blackish patterns on the ground in the landscape when they

Sample	F^-	Cl^-	NO_2^-	Br^-	NO_3^-	PO_4^{3-}	SO_4^{2-}	Σ Anions	Clay [%]
[$mmol_c\ L^{-1}$]									
Black grit	–	1.05	–	–	0.026	0.044	0.138	1.258	3.0
White grit	–	3.24	–	–	0.038	–	0.248	3.526	6.4
Sample	Na^+	NH_4^+	K^+	Mg^{2+}	Ca^{2+}	Σ cations	EC [$\mu S\ cm^{-1}$]	pH	
[$mmol_c\ L^{-1}$]									
Black grit	0.774	0.030	0.265	0.091	0.166	1.326	188	6.9	
White grit	2.761	–	0.322	0.114	3.506	3.506	446	8.0	

Table 1. Anion and Cation Concentration in the 1:10 Aqueous Extract, Electrical Conductivity (EC), and pH of Black and White Grit Samples

are colonized by microorganisms such as lichens. Our study investigated the bioweathering processes mediated by this association of microbial life and the grits, also called grit crust.

Mineralogical Analyses of Black and White Grit Samples (First cm)

The electrical conductivity value observed for the white grit was 2.4-fold higher compared to the black grit (Table 1). Also, the pH-value of the white grit was higher (8.0) compared with that of the black grit (6.9) (Table 1). In the aqueous extracts of the samples, the most common anion was Cl^-, and for the cations Na^+ (Table 1). Comparing black and white grit samples, marked differences existed in the concentration of different anions and cations.

Chemical analysis of the <2 and >2 μm fractions of black and white grits revealed highest SiO_2 contents in the >2 μm fraction, where the primary mineral quartz was typically observed (Table 2). K_2O was highest in the <2 μm fraction indicating that K was not only located in feldspars but also in illite. In this fraction, also the percentage of P_2O_5, Fe, Mn, Cu, and Zn was higher compared to the >2 μm fraction.

For black and white grit samples, diffraction patterns for the <2 μm fraction revealed the presence of illite (peak maximum at 0.99 nm) (Figure 2). In the black grit sample a 2:1 layer silicate phase was indicated by the diffraction peak at 1.40 nm. Traces of kaolinite were indicated by small interferences at 0.713 nm. The presence of relatively high amounts of quartz could be deduced from strong interferences at 0.425 and 0.334 nm. Peak maxima at 0.323 and 0.318 nm could be assigned to feldspars and were most marked in the <2 and >2 μm fraction of the black grit sample. The two clay minerals, typical for arid soils, palygorskite with a strong X-ray diffraction peak at 1.04 to 1.05 nm and sepiolite with a strong maximum at 1.24 nm, were not identified in the samples. Carbonates were absent as well. In the >2 μm samples, the presence of quartz was indicated in addition to the interferences at 0.425 and 0.334 nm by maxima at 0.245 and 0.227 nm. From the SiO_2 content in the >2 μm fractions it was derived that quartz had higher shares in the white grit than black grit sample (77.5 and 68.3% SiO_2, respectively).

Texture and Elemental Composition of the First and Second cm of Substrate and of Dust

The texture of the first and second cm of the analyzed substrate (Figure 3A) was characterized by a high proportion of coarse material (50% > 2 mm), which included the colonized grit stones in the first cm of the profile (Figure 3B). The second cm of the profile mainly consisted of fine material (80% < 2 mm) including 12% of clay-sized particles.

Element contents as gained from inductively coupled plasma – optical emission spectroscopy after acid digestion were normally distributed at $P \leq 0.05$, except for zinc (Zn) which only was normally distributed at $P \leq 0.1$. The total elemental contents of Al, Ca, Fe, Mg, Mn, P, Zn, and C_{inorg} were significantly higher in the second cm compared to the first cm (Figure 3C). The increase in the second cm ranged between 2-fold (Al, Fe) to 7-fold (Ca). The total P content was 3-fold higher in the second cm compared with the first cm. Total C and C_{org}, as well as total N and S were similar in the first and second cm.

Sequential P-fractionation showed that stable P was the dominant P-fraction in both depths. In the second centimeter, its proportion was significantly higher than in the first cm (Figure 3D). Labile and moderately labile P were by trend higher in the first cm.

Sample	MgO	Al_2O_3	SiO_2	P_2O_5	K_2O [%]	CaO	Ti	Fe	Mn	Cu	Zn
Black grit <2 μm	0.54	10.12	47.19	0.074	3.35	0.30	0.149	2.80	0.03	0.022	0.030
Black grit >2 μm	0.78	6.81	68.28	0.025	2.32	0.27	0.082	0.90	0.01	0.003	0.002
White grit <2 μm	0.92	7.32	55.08	0.060	2.52	0.23	0.098	2.20	0.04	0.013	0.019
White grit >2 μm	0.78	4.64	77.51	0.029	1.69	0.23	0.058	0.74	0.02	0.003	0.002

Table 2. Chemical Composition of the <2 μm and >2 μm Fraction

Fluorescence Microscopy of Colonized Grit Stones

Fluorescence microscopy showed black, white and red patterns with black color as the lithomatrix, white color as fluorescence of the fungus due to chitin in the cell walls and red color as chlorophyll fluorescence of the green algae (Figures 4A and 4D). Autofluorescence of green algae would not be visible from dead cells or remnants because chlorophyll rapidly degrades after cell death. Figure 4A demonstrates that lichens grew attached to the surface of the grit stones with single hyphae penetrating the grit. This phenomenon was frequently observed. In addition, most tunnels of single grits were found to be colonized by fungal hyphae and their green algal photobionts even reached the middle of the grits (Figure 4D). Light microscopy of grit thin sections indicated lichen thalli with their green algal photobionts growing tightly attached to the surface of the grit stones. Brown colored cavities beneath the lichens imply clay or Fe-oxides accumulation (Figure 4B). Scanning electron microscopy (SEM) images indicated that the lichen thalli (artificially colored in red) were embedded into the grit surface (artificially colored in green) (Figure 4C).

X-Ray Microtomography

Comparative X-ray microcomputer tomography (μCT) scans of a colonized grit stone in an air-dry status and after 12 hr of hydration revealed a change of lichen structure after wetting. Table 3 shows that the volume of the whole grit (stone including lichen) increased about 21% (Figures 5A and 5B). The volume of the lichen tissue alone, raised up to 55% of its initial value. The relative share of the lichen for the total grit volume increased from 38% in the dry state to 49% when the lichen was hydrated. The fact that the calculated volume of the stone enlarged only very slightly (by 0.13%) is an indicator for the reliability of the μCT data.

The surface area of the whole grit enlarged by 24% (Table 3). This increase is mostly caused by the enlargement of the lichen surface, as the stone surface did expand only by about 2%, which corresponds to the very small increase in the stone's volume. Further, most of the surface expansion happened at the outer surface of the grit. The internal surface area can be calculated when subtracting the surface area of the whole grit from the sum of the surface of mineral phase and lichen, which also have internal surfaces. Interestingly, while the whole grit surface expanded by 24%, the internal surface stayed almost the same with an increase of less than 1% (dry: 677.27 mm^2; wet: 683.69 mm^2).

SEM-energy-dispersive X-ray spectroscopy and Element Composition Analyses

SEM with energy-dispersive X-ray spectroscopy (SEM-EDX) indicated high abundance of Cl and Ca at the external surface of the lichen thalli while mainly potassium K was found at the surface of the grit (Figure 5C). Light microscopy of a thin section of detached lichen thalli revealed high amounts of incorporated mineral particles e.g. iron oxides (brownish colored) within the medulla of the thallus (whitish colored) underneath the photobiont layer (greenish colored) (Figure 5D). Further, SEM images showed mineral particles of varying sizes embedded into the cortex and on top of the lichen thalli (Figure 6A). The elemental composition of these particles included high abundances of Ca and P as revealed by SEM-EDX (Figure 6B). Dust contained mainly Fe and Al but also 0.019 mg P cm^{-2} y^{-1} (Figure 6C).

Long-term pH Measurements of Photobiont Cultures and Enzyme Activity of Colonizing Organisms

During long-term pH measurements of photobiont culture media, a continuous rise in pH from 6.7 up to almost 9 was observed within 12 weeks (Figure 7A). Measurements with the oxygen electrode revealed that all samples containing algal suspensions isolated from single grit crust lichens released oxygen into

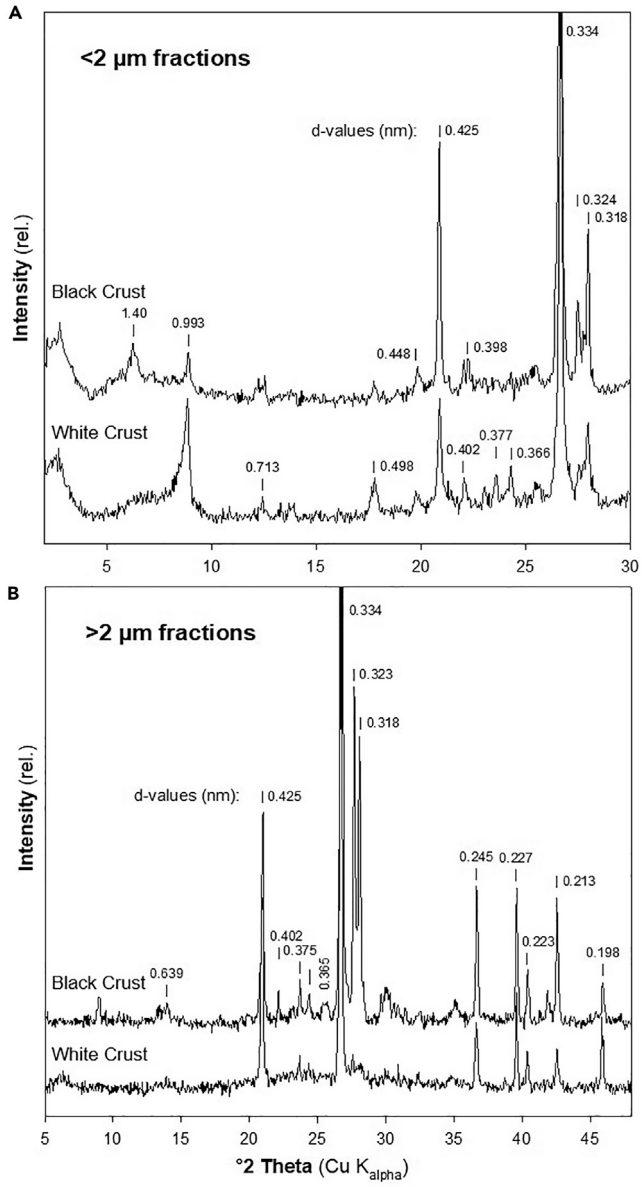

Figure 2. X-ray Diffraction Patterns of the Grit Soil Samples

(A) This represents the <2 µm fraction and (B) the >2 µm fraction of black and white grit samples. Mg-saturated samples were used for the <2 µm fraction.

the medium, and this process was accompanied by increasing alkalization with increasing light levels (Figure 7B). Below a certain light intensity (the so-called compensation point, when photosynthetic oxygen production compensates respiratory oxygen consumption), all samples started to acidify the solution. For all samples, a clear correlation between oxygen uptake/release and the pH was given. All samples alkalized the medium already at relatively low light intensities (<40 µE). Light levels beyond 150 µE caused a saturation in oxygen production. Black grit stones showed mean enzyme activities of 140, 165, and 221 µg p-nitrophenol g^{-1} dw h^{-1} for alkaline phosphatase, acid phosphatase, and phosphodiesterase, respectively (Figure 7C).

DISCUSSION

The availability of water provided by fog, dew, and high air humidity in the region of Pan de Azúcar National Park in the Atacama Desert together with the presence of the grits as a substrate for colonization promotes

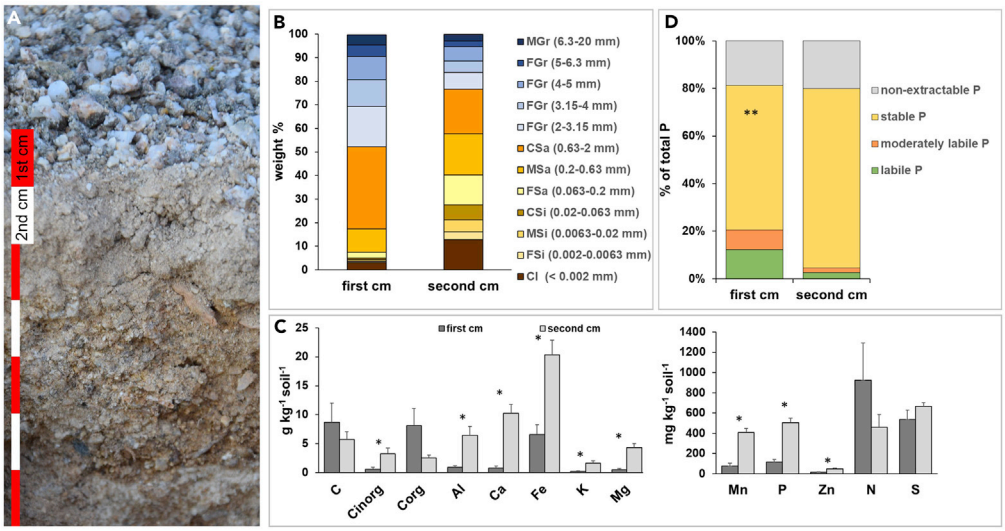

Figure 3. Texture and Elemental Composition of the First and Second Centimeter of a Grit Crust Profile

(A) Upper centimeters of a *terrestrial protopedon* profile with accumulated fine material between and underneath the grit stones; red and white scale bars represent 1 cm each; (B) Texture of the first and second centimeter of the profile; C = coarse, M = middle, F = fine, Gr = gravel, Sa = sand, Si = silt, Cl = clay; (C) Elemental composition of the first and second centimeter of the profile represented as mean +/− standard deviation; asterisks indicate significant differences between an elemental concentration of the first and second centimeter, $p \leq 0.1$, paired t test; (D) P pools as percentage of total P in the first and second centimeter of the profile; asterisks indicate significant differences between first and second centimeter within one fraction at $^{**}p \leq 0.05$, paired t test.

the establishment of the grit crust as a landscape dominating aspect. As a consequence, this unique constellation of microbial life is in turn able to mediate bioweathering processes leading to physicochemical effects on the transformation of rocks. Considering the low amount of available water and relatively low chemical weathering susceptibility of quartz and feldspars in the granitoid rock substrate, biological and physical weathering appear to be the dominating processes during the very initial formation of soil. The large diurnal temperature range, for example (e.g. Jung et al., 2019a), causes thermal stress (insolation weathering) in the granitoid particles as differences in mineral expansion set up cause the polycrystalline rocks to crack preferentially at grain boundaries (Vasile and Vespremeanu-Stroe, 2017) which offers a great ecological niche for microbes of any kind. However, the bioweathering processes on which this study focused were those mediated by lichens, cyanobacteria and fungi that support the deterioration of rocks from a microscope to the landscape perspective and from the rock to the fine substrate as depicted in a possible chronosequence in Figure 1. However, the investigated and described processes are just observed in nature, as a result at the time of the sampling, not by following the course of development. Below several bioweathering processes such as enzyme activity, pH alterations, the incorporation of mineral fragments, shrinking-swelling activity of whole colonized grits and the re-localization of mineral fragments will be discussed on basis of the scheme summarized in Figure 8.

Pore Spaces in Grit Particles

A common observation in thin sections of black grit samples was the presence of large pore systems (Figures 3D, 4A, and 4B), which were connected and open to the external surface (Jung et al., 2020), thus presenting a potential prerequisite for e.g. internal weathering reactions (Dultz et al., 2006). These pore systems may be the result of two different processes: (1) The pore system could at least in parts represent relicts of previous fluid-rock interactions, which took place e.g. in the hydrothermal phase after formation of the bedrock plutonite from which the granitoid grit particles originated. For the formation of cracks, fracturing during cooling of the plutonite, pressure relief by erosion and insolation weathering has to be considered (Wiggering, 1987). During dissolution of the minerals, a marked share of the parent material could have been lost to the liquid phase, hereby increasing the porosity (Putnis, 2002). The formation and precipitation of secondary phases (clay minerals and sesquioxides) may have counteracted this effect, in particular if elements were supplied from the surrounding solution. The presence of clay minerals in the

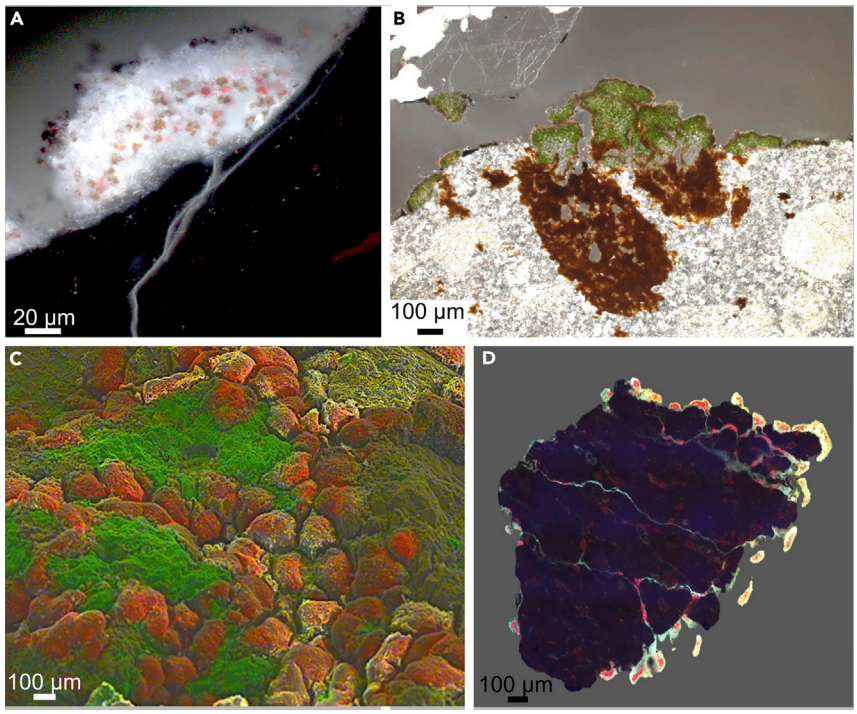

Figure 4. Evidence for Penetration of the Lithomatrix by Lichens

(A) Fluorescence microscopy of grit stone showing fungal hyphae (white; chitin autofluorescence) penetrating the grit surface and green algal photobionts (red; chlorophyll autofluorescence) indicating the microstructures that potentially lead to a deterioration of the grit stones; (B) Light microscopy of grit cross section with lichen thalli (green) and cavities filled with brown particles underneath that demonstrate that lichens accumulate fine material; (C) Artificially colored SEM image with lichen thalli (red) embedded into the grit (green) showing that the lichen thalli are embedded into the surface of the grits; (D) Fluorescence microscopy of whole grit stone showing fungal hyphae (white; chitin autofluorescence) and green algal photobionts (red; chlorophyll fluorescence) inside of a grit stone. SEM, scanning electron microscopy.

pore system could have slowed down chemical weathering reactions as the surface of primary minerals could have been covered and pore diameters could have been narrowed by clay-sized particles. (2) Existing cracks can enable large diameter dissolution reaction by microbial colonization and relatively fast convective transport (Dultz et al., 2013) that may also have contributed to the observed pore system of the grit stones.

Penetration of the Lithomatrix by Lichens

In Pan de Azúcar, lichen thalli established at the surface of granitoid substrate particles (Figure 4A), probably used the enhanced water condensation properties of the quartz containing substrate in a similar way as it was described for cyanobacteria by Azúa-Bustos et al. (2011). Once established, it can be speculated that the lichen started to alter the lithomatrix by drilling into the grit (Figure 8, gray hyphae inside grit) causing tramlines (superficial grooves) and channel formation on the surface, as well as cuts, holes, and borings (Figure 4D). These processes have been described in many other studies (e.g. Adamo and Violante, 2000). Often a significant pH reduction in the vicinity of cells upon mineral surface attachment or a significant turgor pressure of around 10–20 MPa that is applied toward the lithomatrix can be observed (Howard et al., 1991). This can lead to mineral mass loss at the interface of lithomatrices causing pits and tramlines. Those mass losses were estimated to account for ~40%–50% of the overall bioweathering (Li et al., 2016). Additionally, the excretion of siderophores is also a common bioweathering strategy for microbes to overcome Fe deficiency (due to the strong tendency of Fe^{3+} to precipitate at circum-neutral pH). Siderophores chelate Fe-ions which can also lead to the dissolution of the lithomatrix (Neilands, 1995; Li et al., 2016). Near surface structures were found such as the brownish appearing material which was assigned to vermiculite or smectite clay minerals in combination with Fe-oxyhydroxides. These were interpreted as neoformations and are thus stable in longer terms due to the high insolubility of Al-dominated and Fe-dominated minerals

	Dry		Wet		% change	
	Volume [μL]	Surface area [mm^2]	Volume [μL]	Surface area [mm^2]	Volume	Surface area
Stone	41.21	453.70	41.26	461.52	±0.13	±1.73
Lichen	25.75	653.31	39.99	756.82	±55.29	±15.84
Whole grit	66.96	429.75	81.26	534.66	±21.35	±24.41

Table 3. Results of the Microcomputed Tomography Analysis

Volume and surface area of the colonized grit components (stone and lichen) and whole grit before and after wetting. Note that the surface area of the whole grit is only referring to the outer surfaces.

at neutral pH (Banfield et al., 1999). Similar drilling processes and traces have been observed for a variety of fungi growing on e.g. limestone (Burford et al., 2003a, 2003b), but it remains unanswered if the grit crust organisms are actively causing the cracks or if they start growing at preexisting fissures. Evidence of a siderophore related bioweathering can be found in a significant enrichment of Fe in the second cm of the grit crust (Figure 3C) what might be the consequence of accumulated fine material.

The observed tunnels were not only colonized by fungi but also by phototrophs reaching deep inside of grits (Figures 4D and 8 gray hyphae and green photobionts inside the grits). Interestingly they were able to maintain their photosynthetic activity inside the grits due to the translucent character of the grits. With time, the lichen thalli then could invade the stone, which can be observed as embedded thalli (Figure 4C). This can lead to a direct contact even between the green algal photobionts in inner parts of the lichen thalli and the lithomatrix promoting additional types of bioweathring processes (Figure 8, inlet).

Alkalinolysis, Acidification and Enzyme Activity of Grit Crust Communities

The pH-value of the white grit was higher (8.0) compared with that of black (i.e. = densely colonized) grit (6.9) (Table 1) indicating that the microorganisms might induce chemical weathering through the release of protons and organic acids.

Interestingly, the complementary experiments with the isolated photobionts of the lichens showed that trebouxioid green algae could increase the pH of a culture medium in the short-term, as well as in the long-term and that this was related to their photosynthetic activity (Figures 7A and 7B). During photosynthesis, green algae excrete OH^- as a byproduct, which in turn alkalizes the medium, a process known as alkalinolysis (Figure 8, inlet). This appears as a contradiction to the lower total pH of the black grit compared to the white grit but one needs to take into consideration that experiments with the isolated photobionts need to be interpolated to the *in situ* situation with care: for these experiments a high amount of biomass was required that cannot be found in nature to a comparable extend. Nevertheless, the process of alkalinolysis can be transferred to lichens because the photobionts were able to increase the pH in the experiments which means it is likely that they could do this in the lichens as well even during short terms of activity induced by e.g. fog (Jung et al., 2019a). This will result in alkalinolysis effects on the microscale where, e.g., a quartz fragment is stuck in the lichen thallus touching a few photobionts, which was indeed observed (Figure 5D). This will not cause a high pH in a bulk sample of several grams but a high pH at a certain spot within the lichen thallus, close to such a mineral fragment. These alkalinolysis processes have been described mainly for trebouxioid green algae (Shiraiwa et al., 1993; Weber et al., 2011) and some cyanobacteria such as *Chroococcidiopsis* (Büdel et al., 2004). These genera were found among the grit crust community (Jung et al., 2020). Interestingly, quartz as the main compound of the grit dissolves at pH > 7.5 (Brundsen, 1979) because here the solubility of mainly Si strongly increases, what could happen during alkalinolysis in the interface between photobionts and the lithomatrix of the grits.

In contrast to alkalinolysis, Salvadori and Municchia (2016) reviewed several acidic metabolites excreted by lichens and fungi as main weathering agents but also stated that this is depending on the lichen species and the climate. Although we did not detect any acidification reactions in our experiment with green algae, it is still possible that the fungal part of the lichen, the multicolonial fungi or other heterotrophic microorganisms can excrete acids or lichen compounds to deteriorate specific minerals within the grit stones.

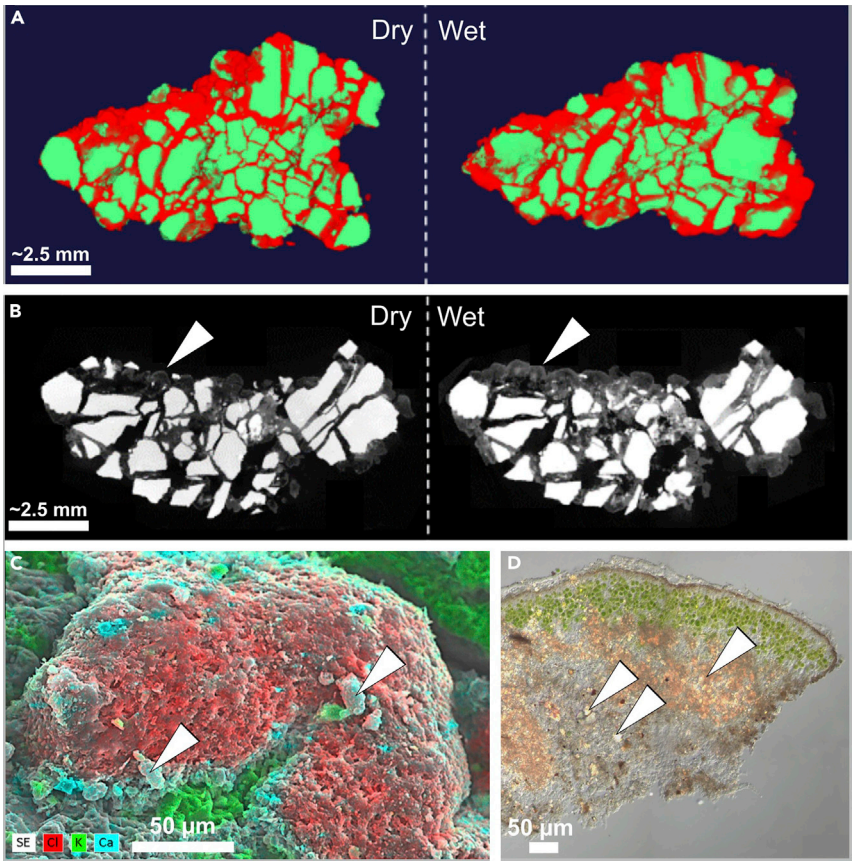

Figure 5. Effects of Fog and Dew Induced Wet-Dry Cycles and Mineral Accumulation on Colonized Black Grit

(A) Schematic output of the segmented 3D model for the grit before (left) and after wetting (right). While the stones (green) did not change their volume, the lichen tissue (red) showed a considerable increase in volume, which is especially obvious for the inner regions between the stone fragments.

(B) Gray scale tomograms of the grit before (left) and after wetting (right). Arrows indicate regions where swelling of the lichen tissue was most pronounced.

(C) Artificially colored SEM-EDX image showing the presence of salts attached to a lichen thallus (arrowheads); (D) Microscopic cross section of lichen thallus showing incorporated minerals (arrowheads) as weathered residues. SEM, scanning electron microscopy; EDX, energy-dispersive X-ray spectroscopy.

Interestingly, enzyme assays revealed a comparably high activity of alkaline, acidic and diester-phosphatases (Figure 7C), which indicates that both processes, alkalization as well as acidification may have happened simultaneously but at different micro-sites. This may be explained by (i) the polycrystalline lithomatrix of the grit stones causing a scattered pattern of minerals with different probabilities of pH-shifts into the one or the other direction and (ii) the diverse taxonomic composition of the grit crust community which is not yet fully characterized.

Wet-Dry Cycles

The arid component of the National Park is interrupted by fog and dew providing water for organisms (Lehnert et al., 2018). This constantly causes several wet-dry cycles per day (Jung et al., 2020). Poikilohydric organisms, such as lichens, cyanobacteria green algae and other heterotrophic microorganisms are able to use even these short periods of water availability e.g. with the help of excreted extracellular polymeric substances (EPSs). Swelling and shrinking movements of the organisms (Figure 8, whitish symbols) can cause or at least reinforce mechanical disruption of the lithomatrix. Our observations showed that a single grit stone colonized by lichens increased its volume by 21% upon wetting compared to air-dry conditions, with the lichen tissue alone increasing its volume by 55% (Figures 5A and 5B and Table 3). This demonstrates the high fragmentation potential of the microhabitat caused by the organisms in dependency of water input.

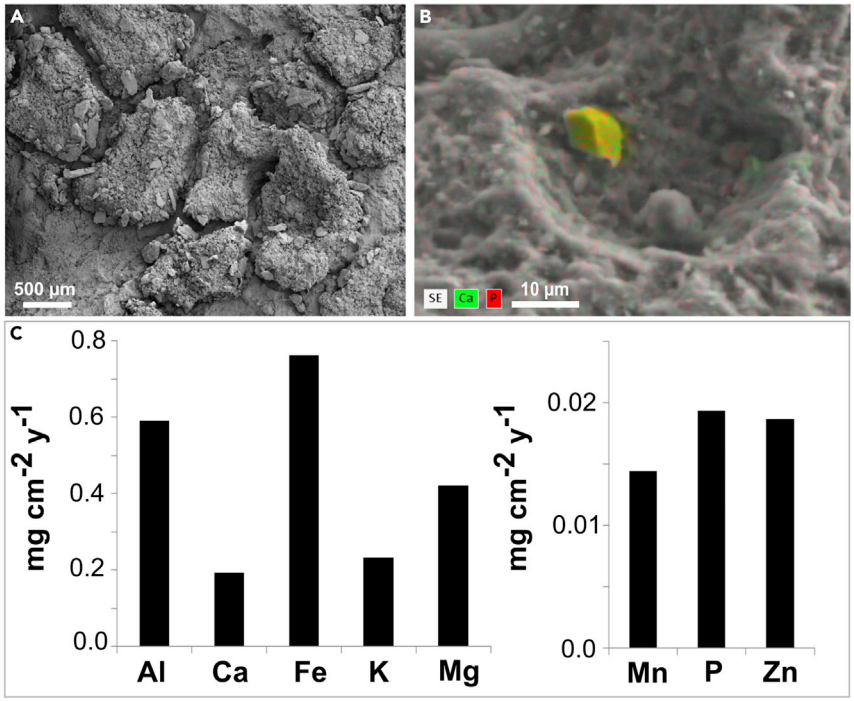

Figure 6. Mineral Accumulation on Grit Surface and Elemental Dust Composition

(A) SEM image of lichen thalli attached to grit with mineral particles from dust on the cortex of the thalli; (B) Artificially colored close-up SEM-EDX image of dust particle on top of lichen thalli showing a grain consisting of Ca and P compounds; (C) Elemental deposition by dust. SEM, scanning electron microscopy; EDX, energy-dispersive X-ray spectroscopy.

Pure lichen thalli were reported to have water holding capacities up to 300% of their dry weight (Creveld, 1981), highlighting the deteriorating potential of lichens within such a system. The analysis of the surface area revealed that its increase occurred mainly at the surface of the grit (that is, of the lichen), while the (internal) interface of lichen and stone increased by less than 1%. One possible explanation for this pattern could be that the biomass of the organisms was probably much higher at the surface of the grits than in the internal structures. This was supported by fluorescence microscopy of grit cross sections showing a loose fungal network together with only a few green algae (Figure 4D). Here, the forces applied by shrinking and swelling were probably much weaker, but as the fog and dew events are cyclic on a regular basis a deterioration over time is likely. Meteorological records of the sampling sites for example showed that dew occurred frequently, predominately during night-time providing between 0.025 and 0.088 mm of liquid water per day but fog usually occurred during daytime providing higher water fluxes delivering 0.38–1.25 mm per day (Jung et al., 2020). However, it should be stressed that the lichens in our laboratory study were completely submerged in water for 10 min and then were given time to equilibrate overnight (12 h). It is possible that the behavior of the lichens would be somewhat different if they were subjected to the realistic environmental conditions (with water droplet supply from the gaseous phase) that they usually experience in the field.

In order to get a better understanding of the actual processes that are occurring in the field, a more sophisticated experimental design will be necessary in future studies. For example, the simulation of a changing water availability during dew or fog events would be possible with an environmental chamber such as the one described by Raanan et al. (2016). This would allow the quantification of the grit crust's structural dynamics during and at the end of fog or dew events in the Atacama Desert. For example, biological disruption of grits can be enhanced by the crystallization of salts within pores and cracks within the lithomatrix (Wellman and Wilson, 1965). Here analysis of the aqueous extract revealed distinct amounts of soluble salts in the samples (Table 1). In addition we observed Ca-containing phases accumulated next to the lichen thalli (Figure 5C), whereby the Ca might originate from dissolution of minerals. Inside the grit stones,

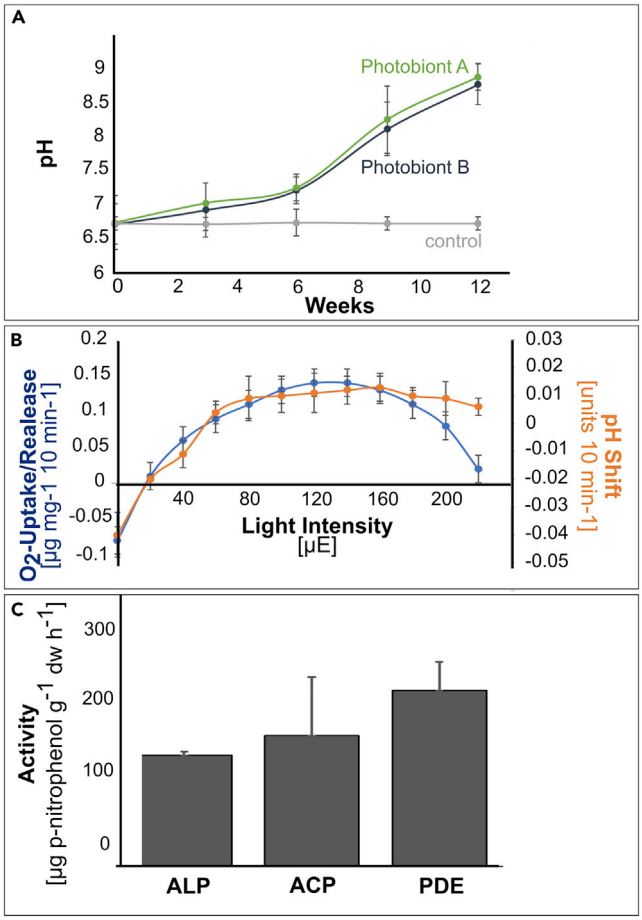

Figure 7. Alkalinolysis and Enzyme Activity of Grit Organisms

(A) Long-term incubation of two isolated green algal photobionts (n = 3, for each photobiont and the control) indicating a raise in pH over the course of 12 weeks; (B) Short-term experiment with isolated green algal photobionts (n = 6) showing pH shifts depending on oxygen production during varying light conditions; (C) Enzyme activity of alkaline phosphatases (ALP), acidic phosphatases (ACP), and phosphodiesterases (PDE) (n = 3). Data represent mean +/− standard deviation.

Ca-containing P compounds may have been solubilized in water, ions been transported along the fungal network before mineral re-crystallization within the lichen thalli or the lichen's cortex as a consequence of evapotranspiration (Figure 8, brownish and blueish arrow) (Banfield et al., 1999). Further, this Ca-enrichment also could be a consequence of carbonatization performed by cyanobacteria or green algae.

Mineral Accumulation

Besides Ca-containing compounds on top of the lichen thalli, mineral fragments were also found to be incorporated into the lichen thalli (Figure 4B). This was already described as mechanical action of crustaceous lichens on shale, shist, gneiss, limestone and obsidian by Fry, 1927. Barker and Banfield (1996) found that mineral fragments as small as 5 µm were incorporated into the lower thallus of lichens as a consequence of bioweathering processes on amphibole syenite. Further, we observed airborne dust particles which were embedded into the cortex of the thalli and which were concatenated by the fungal hyphae and EPS (Figures 6A, 6B, and 8, triangles on lichen's surface). Recently, it could be shown that up to 4 g m^{-2} of dust can accumulate at comparable sites in the Atacama Desert already within one month (Azua-Bustos et al., 2019). Comparable dust inputs have been shown to be trapped by cryptogamic ground covers of the Colorado Plateau enriching the soils with P, Mg, Na, K, Mo, and Ca thus highlighting the role of these surface consortia in fueling nutrient cycles (Reynolds et al., 2001). Dust at the Pan de Azúcar sampling site mainly consisted of Fe and Al containing compounds (Figure 6C) suggesting that these compounds

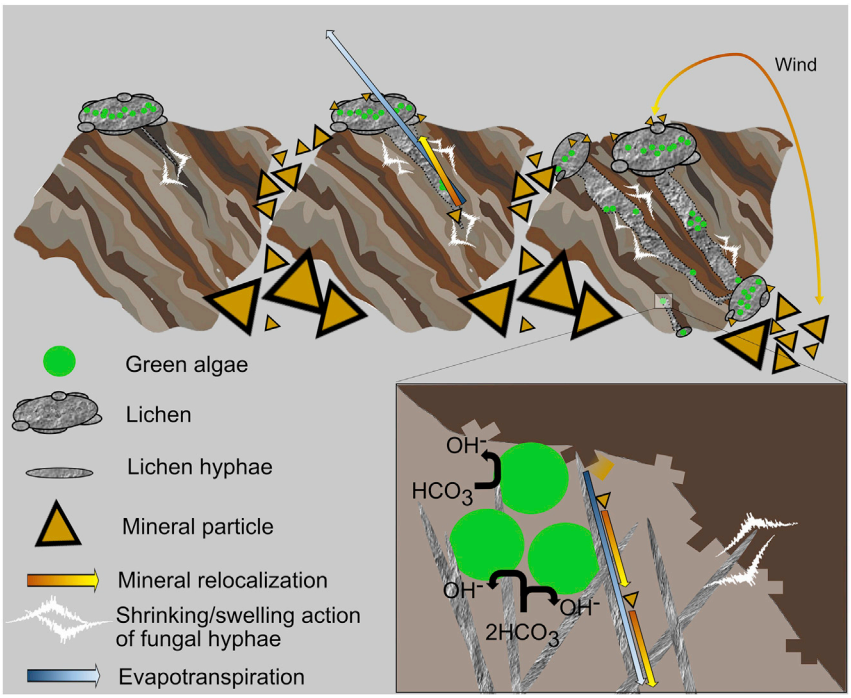

Figure 8. Schematic Overview of Bioweathering Processes

Lichens consisting of a mycobiont and its hyphae (gray) together with green algal photobionts (green) colonize polycrystalline grit stones (brown tones) that have a size of roughly 6 mm. The hyphae of the lichen penetrate the lithomatrix causing tunnels induced by shrinking and swelling actions (white arrow) induced by fog and water input that hydrate the lichen. Further bioweathering activity (depicted in the inlet) leads to solubilization of minerals during times of hydration as a consequence of photosynthetic activity of the green algae photobionts. These excrete OH^- as a byproduct into the lithomatrix which causes alkalization that can promote the dissolution of e.g. quartz and other minerals. These minerals can be relocated (yellow arrow) following the direction of evapotranspiration (blue arrow) and re-crystallize (yellow triangles) on the surface of the lichen. On the surface of the lichens which is sticky due to excreted mucus like substances, mineral particles can accumulate between the grit stones from where they can be re-transported by wind (yellow arrow) which in turn can also lead to the accumulation of fine material on the lichen's surface.

probably originated from weathering products that were transported via dust over more or less long distances and thus could also be due to mining activities in the vicinity.

Nutrient elements such as P were part of the dust particles and co-occurred with Ca (Figure 6B) implying the presence of apatite ($Ca_5(PO_4)_3(F,Cl,OH)$). Different lichen species interacting with apatite that carries P, one of the most growth-limiting elements in arid ecosystems (Zhao and Zeng, 2005), have recently been reported by Baumann et al. (2018) from another experimental site that was close to the sampling site of the present study.

Pedogenesis and Accumulation of Available P

In the field, we observed that colonized grit stones were located on top of finer substrate (Figure 3A). Texture analysis revealed that almost 70 weight % in the second cm were substrate particles <2 mm (Figure 3B). We assume that this is a consequence of grit weathering during which parts of the lithomatrix broke off in the first cm and deposited as second centimeter (Figure 8, triangles). Further, deposition of secondary minerals may have contributed, as lichens were shown to be especially effective in altering feldspars to clay minerals or clay-sized particles even if this was the result of a long-term effect (Jackson, 2015). This is supported by significantly higher elemental concentrations of almost all investigated elements underneath the grits (Figure 3C). The enrichment in elements was also found for P, mainly occurring as relatively stable P (Figure 3D), which may include e.g. apatite- and phythate-P, as well as P occluded within sesquioxides (Baumann et al., 2018). These P-sources meet special demands of microorganisms as P supply is known to be one of the limiting factors for biological growth in arid ecosystems (Zhao and Zeng, 2005).

However, total C, C_{org} and N were only tendentially higher in the first compared with the second centimeter of the profile although the biomass of at least the phototrophic organisms was visibly concentrated in the first centimeter. In general, N accumulates in phototrophic communities because of the N fixing abilities of heterocytous cyanobacteria (Elbert et al., 2012), which were also found among the grit crust community (Jung et al., 2019b, 2020).

Also, the C_{org} concentration as a biomass proxy indicated similar biomass for both centimeters, which could be due to a vivid phototrophic community in the first centimeter and a well-established community of mainly heterotrophs in the second centimeter. In contrast, C_{inorg} was significantly higher in the second centimeter, which is in line with higher concentrations of Ca-containing compounds. They may have originated from grit stone weathering and/or dust deposition. Total C concentration, comprising C_{org} and C_{inorg} was highly variable and thus similar between the first and second centimeter. In addition, wind erosion in the Atacama Desert (McKay et al., 2003), leading to substrate input and output, may have affected elemental concentrations in both centimeters. However, the enrichment of fine particles appears to be the sum of (among others) bioweathering actions such as alkalinolysis of the lichen photobionts, drilling of the lichen's hyphae, dust trapping of biopolymers such as EPS and shrinking/swelling actions of microorganisms in internal structures of the lithomatrix. The bioweathering of rock material over time led to the formation of a *terrestrial protopedon* (Figure 8, triangles on the right side) (Jung et al., 2020), a young soil named in analogy to similarly young soils in aquatic ecosystems that are rich in $CaCO_3$ with high contents of sand, silt or clay but which are poor in organic C (Amelung et al., 2018).

Landscape Scenario and Significance

Considering that the climate of the Atacama Desert has been stable for 150 million years (Hartley at al. 2005) together with the ancient origin of lichens and algae it can be speculated that all of the described and simultaneously occurring weathering processes are part of an ongoing dynamic that takes place over geological timescales. Following this, the deterioration of rocks leads to the formation of smaller rocks over the formation of grits and finally to the terrestrial protopedon as a chronosequence (Figure 1). This appears to be a significant geomorphological process in parts of the Atacama Desert fueled by a community of microorganisms such as those of the grit crust. In this sequence the colonized grits could be seen as a snapshot of the present bioweathering stage at least in the landscape of Pan de Azúcar or there where the grit crust will be detected in future. Although this study focused mainly on lichens, algae and fungi it should be stressed that they are by far not the only active microorganisms in this system. Even a single lichen nowadays needs to be understood as a self-sustaining ecosystem formed by the interaction of an exhabitant fungus and an extracellular arrangement of one or more photosynthetic partners and an indeterminate number of other microscopic organisms (Hawksworth and Grube, 2020). Nevertheless we tried to assign specific bioweathering processes to single types of organisms because there are always surprises: recently, the extreme thermoacidophile *Metallosphaera sedula*, a metallophilic archaeon, was found to thrive on meteorite minerals (Milojevic et al., 2019) and other examples are *Manganitrophus noduliformans* and *Ramlibacter lithotrophicus* that were the first organisms that helped to untangle the mechanisms behind chemolithoautotrophy via manganese oxidation (Yu and Leadbetter, 2020). The great and so far unstudied diversity of microorganisms that are part of the grit crust biocenosis in the Atacama Desert might therefore be an interesting source for further bioweathering studies.

Limitations of the Study

The authors want to clearly state that this study aims to give an overview on various interactions between the lithomatrix and different microbes without quantitatively investigating single processes. Only a very high number of replicates for each of the single weathering processes could be upscaled to the landscape scale at which they are taking place and at which several follow-up studies should focus in future. One of these studies will focus on a method to detect the shrinking and swelling actions of the grits induced by fog and dew mimicking more natural conditions in contrast to the lab-based approach of this study.

The contribution of this study also ends at untangling the detailed community structure of the grit crust and therewith cannot account for bioweathering activities of e.g. heterotrophic bacteria. Further, the degree to which dust deposition, local physical weathering, or the mining activity in the area contribute to the finer substrate layer could not be resolved here.

Resource Availability

Lead Contact

Requests for materials and communications with the journal should be addressed to Patrick Jung (patrick_jung90@web.de).

Materials Availability

This study did not generate new unique reagents.

Data and Code Availability

All datasets used for this study are accessible through the lead author Patrick Jung (patrick_jung90@web.de).

METHODS

All methods can be found in the accompanying Transparent Methods supplemental file.

SUPPLEMENTAL INFORMATION

Supplemental Information can be found online at https://doi.org/10.1016/j.isci.2020.101647.

ACKNOWLEDGMENTS

This work was funded by the German Research Foundation Priority Program 1803 "EarthShape: Earth Surface Shaping by Biota" in the frame of the project CRUSTWEATHERING (BU666/19-1, LE903/14-1). Some of the research was performed within the scope of the Leibniz ScienceCampus "Phosphorus Research Rostock". The authors thank Prof. Stephan Peth for giving them access to the tomography lab of the University of Kassel. The authors would like to thank B. Balz and E. Heilmann (Soil Science, University of Rostock) for element extraction and ICP-OES analyses, Nora Vitow for enzyme activity analyses (Soil Science, University of Rostock), as well as the Chilean National Park Service (CONAF) for providing access to the sample locations and on-site support of the research. P.J. thanks the EFRE project PHOTOPROMA for funding.

AUTHOR CONTRIBUTIONS

P.J., B.B., K.B., and P.L. conceived the study; K.B. and P.J. collected all samples; P.J. and D.E. conducted the pH measurements of the photobionts; K.B. analyzed and calculated soil and dust data while S.D. performed mineralogical analyses; A.S. and M.F. took REM-EDX images; C.B. analyzed the enzyme activity; V.F. prepared and analyzed the μCT images; P.J. and K.B. wrote the manuscript with input and editing from all other co-authors.

DECLARATION OF INTERESTS

The authors declare no competing interests.

Received: June 11, 2020
Revised: September 25, 2020
Accepted: October 1, 2020
Published: November 20, 2020

REFERENCES

Adamo, P., and Violante, P. (2000). Weathering of rocks and neogenesis of minerals associated with lichen activity. Appl. Clay Sci. *16*, 229–256.

Amelung, W., Blume, H.-P., Fleige, H., Horn, R., Kandeler, E., Kögel-Knabner, I., Kretschmar, R., Stahr, K., and Wilke, B.-M. (2018). Scheffer/Schachtschabel Lehrbuch der Bodenkunde. 17 (Auflage. Heidelberg).

Azua-Bustos, A., González-Silva, C., Fernández-Martínez, M.Á., Arenas-Fajardo, C., Fonseca, R., Martín-Torres, F.J., and Zorzano, M.P. (2019). Aeolian transport of viable microbial life across the Atacama Desert, Chile: implications for Mars. Sci. Rep.-UK *9*, 1–11.

Azúa-Bustos, A., González-Silva, C., Mancilla, R.A., Salas, L., Gómez-Silva, B., McKay, C.P., and Vicuña, R. (2011). Hypolithic cyanobacteria supported mainly by fog in the coastal range of the Atacama Desert. Microb. Ecol. *61*, 568–581.

Banfield, J.F., Barker, W.W., Welch, S.A., and Taunton, A. (1999). Biological impact on mineral dissolution: application of the lichen model to understanding mineral weathering in the rhizosphere. Proc. Natl. Acad. Sci. U S A *96*, 3404–3411.

Barker, W.W., and Banfield, J.F. (1996). Biologically versus inorganically mediated weathering reactions: relationships between minerals and extracellular microbial polymers in lithobiontic communities. Chem. Geol. *132*, 55–69.

Baumann, K., Jung, P., Samolov, E., Lehnert, L.W., Büdel, B., Karsten, U., and Oses, R. (2018). Biological soil crusts along a climatic gradient in Chile: richness and imprints of phototrophic microorganisms in phosphorus biogeochemical cycling. Soil Biol. Biochem. *127*, 286–300.

Belnap, J. (2003). The world at your feet: desert biological soil crusts. Front. Ecol. Environ. *1*, 181–189.

Beraldi-Campesi, H., Hartnett, H.E., Anbar, A., Gordon, G.W., and Garcia-Pichel, F. (2009). Effect of biological soil crusts on soil elemental concentrations: implications for biogeochemistry and as traceable biosignatures of ancient life on land. Geobiology *7*, 348–359.

Burford, E.P., Fomina, M., and Gadd, G.M. (2003a). Fungal involvement in bioweathering and biotransformation of rocks and minerals. Mineralogical Mag. *67*, 1127–1155.

Burford, E.P., Kierans, M., and Gadd, G.M. (2003b). Geomycology: fungi in mineral substrata. Mycologist *17*, 98–107.

Brundsen, D. (1979). Weathering. In Process in Geomorphology, C. Embleton and T.J. Edward Arnold, eds. (London: Press), pp. 73–129.

Büdel, B., Weber, B., Kühl, M., Pfanz, H., Sültemeyer, D., and Wessels, D. (2004). Reshaping of sandstone surfaces by cryptoendolithic cyanobacteria: bioalkalization causes chemical weathering in arid landscapes. Geobiology *2*, 261–268.

Chen, J., Blume, H.P., and Beyer, L. (2000). Weathering of rocks induced by lichen colonization—a review. Catena *39*, 121–146.

Creveld, M. (1981). Epilithic lichen communities in the alpine zone of Southern Norway. Bibliotheca Lichenologica 17 (J Cramer), p. 287.

Daghino, S., Martino, E., and Perotto, S. (2010). Fungal weathering and implications in the solubilization of metals from soil and from asbestos fibres. In Current Research, Technology and Education Topics in Applied Microbiology and Microbial Biotechnology, A. Mendez-Vilas, ed. Badajoz: Formatex Research Center, pp. 329–338.

Dultz, S., Simonyan, A.V., Pastrana, J., Behrens, H., Plötze, M., and Rath, T. (2013). Implications of pore space characteristics on diffusive transport in basalts and granites. Environ. Earth Sci. *69*, 969–985.

Dultz, S., Behrens, H., Simonyan, A., Kahr, G., and Rath, T. (2006). Determination of porosity and pore connectivity in feldspars from soils of granite and saprolite. Soil Sci. *171*, 675–694.

Dümig, A., Veste, M., Hagedorn, F., Fischer, T., Lange, P., Spröte, R., and Kögel-Knabner, I. (2014). Organic matter from biological soil crusts induces the initial formation of sandy temperate soils. Catena *122*, 196–208.

Elbert, W., Weber, B., Burrows, S., Steinkamp, J., Büdel, B., Andreae, M.O., and Pöschl, U. (2012). Contribution of cryptogamic covers to the global cycles of carbon and nitrogen. Nat. Geosci. *5*, 459–462.

Fry, E.J. (1927). The mechanical action of crustaceous lichens on substrata of shale, schist, gneiss, limestone, and obsidian. Ann. Bot. *41*, 437–460.

Garcia-Pichel, F., Felde, V.J.M.N.L., Drahorad, S.L., and Weber, B. (2016). Microstructure and weathering processes within biological soil crusts. In Biological Soil Crusts: An Organizing Principle in Drylands, *226*, B. Weber, B. Büdel, and J. Belnap, eds (Springer), pp. 237–255.

Hawksworth, D.L., and Grube, M. (2020). Lichens redefined as complex ecosystems. New Phytol. *227*, 1281–1283.

Howard, R.J., Ferrari, M.A., Roach, D.H., and Money, N.P. (1991). Penetration of hard substrates by a fungus employing enormous turgor pressures. Proc. Natl. Acad. Sci. U S A *88*, 11281–11284.

Jackson, T.A. (2015). Weathering, secondary mineral genesis, and soil formation caused by lichens and mosses growing on granitic gneiss in a boreal forest environment. Geoderma *251–252*, 78–91.

Jung, P., Baumann, K., Lehnert, L.W., Samolov, E., Achilles, S., Schermer, M., Karsten, U., and Büdel, B. (2020). Desert breath—How fog promotes a novel type of soil biocenosis, forming the coastal Atacama Desert's living skin. Geobiology *18*, 113–124.

Jung, P., Emrich, D., Briegel-Williams, L., Schermer, M., Weber, L., Baumann, K., Bendix, J., and Büdel, B. (2019a). Ecophysiology and phylogeny of new terricolous and epiphytic chlorolichens in a fog oasis of the Atacama Desert. MicrobiologyOpen *8*, e894.

Jung, P., Schermer, M., Briegel-Williams, L., Baumann, K., Leinweber, P., Karsten, U., and Büdel, B. (2019b). Water availability shapes edaphic and lithic cyanobacterial communities in the Atacama Desert. J. Phycol. *55*, 1306–1318.

Kirtzel, J., Ueberschaar, N., Deckert-Gaudig, T., Krause, K., Deckert, V., Gadd, G.M., and Kothe, E. (2020). Organic acids, siderophores, enzymes and mechanical pressure for black slate bioweathering with the basidiomycete Schizophyllum commune. Environ. Microbiol. *22*, 1535–1546.

Lehnert, L.W., Thies, B., Trachte, K., Achilles, S., Osses, P., Baumann, K., and Karsten, U. (2018). A case study on fog/low stratus occurrence at Las Lomitas, Atacama Desert (Chile) as a water source for biological soil crusts. Aerosol Air Qual. Res. *18*, 254–269.

Li, Z., Liu, L., Chen, J., and Teng, H.H. (2016). Cellular dissolution at hypha-and spore-mineral interfaces revealing unrecognized mechanisms and scales of fungal weathering. Geology *44*, 319–322.

Lumbsch, H. T., & Rikkinen, J. (2017). 4 Chapter Evolution of Lichens. The fungal community: its organization and role in the ecosystem 53.

Matlakowska, R., Skłodowska, A., and Nejbert, K. (2012). Bioweathering of Kupferschiefer black shale (Fore-Sudetic Monocline, SW Poland) by indigenous bacteria: implication for dissolution and precipitation of minerals in deep underground mine. FEMS Microbiol. Ecol. *81*, 99–110.

McKay, C.P., Friedmann, E.I., Gómez-Silva, B., Cáceres-Villanueva, L., Andersen, D.T., and Landheim, R. (2003). Temperature and moisture conditions for life in the extreme arid region of the Atacama Desert: four years of observations including the El Nino of 1997–1998. Astrobiology *3*, 393–406.

Mergelov, N., Mueller, C.W., Prater, I., Shorkunov, I., Dolgikh, A., Zazovskaya, E., and Goryachkin, S. (2018). Alteration of rocks by endolithic organisms is one of the pathways for the beginning of soils on Earth. Sci. Rep.-UK *8*, 1–15.

Milojevic, T., Kölbl, D., Ferrière, L., Albu, M., Kish, A., Flemming, R.L., and Schleper, C. (2019). Exploring the microbial biotransformation of extraterrestrial material on nanometer scale. Sci. Rep.-UK *9*, 1–11.

Mitchell, R.L., Strullu-Derrien, C., and Kenrick, P. (2019). Biologically mediated weathering in modern cryptogamic ground covers and the early Paleozoic fossil record. J. Geol. Soc. *176*, 430–439.

Neilands, J.B. (1995). Siderophores: structure and function of microbial iron transport compounds. J. Biol. Chem. *270*, 26,723–726.

Nelsen, M.P., Lücking, R., Boyce, C.K., Lumbsch, H.T., and Ree, R.H. (2020). The macroevolutionary dynamics of symbiotic and phenotypic diversification in lichens. Proc Natl Acad Sci U S A *117*, 21495–21503.

Ortega-Morales, B.O., Narváez-Zapata, J., Reyes-Estebanez, M., Quintana, P., la Rosa-García, D., Bullen, H., and Chan-Bacab, M.J. (2016). Bioweathering potential of cultivable fungi associated with semi-arid surface microhabitats of Mayan buildings. Front. Microbiol. *7*, 201.

Putnis, A. (2002). Mineral replacement reaction: from macroscopic observatiobs to microscopic mechanism. Mineralog. Mag. *66*, 698–708.

Raanan, H., Oren, N., Treves, H., Berkowicz, S.M., Hagemann, M., Pade, N., and Kaplan, A. (2016). Simulated soil crust conditions in a chamber system provide new insights on cyanobacterial acclimation to desiccation. Environ. Microbiol. *18*, 414–426.

Reynolds, R., Belnap, J., Reheis, M., Lamothe, P., and Luiszer, F. (2001). Aeolian dust in Colorado Plateau soils: nutrient inputs and recent change in source. Proc. Natl. Acad. Sci. U S A *98*, 7123–7127.

Salvadori, O., and Municchia, A.C. (2016). The role of fungi and lichens in the biodeterioration of stone monuments. Open Conf. Proc. J. *7*, 1–34.

Shiraiwa, Y., Goyal, A., and Tolbert, N.E. (1993). Alkalization of the medium by unicellular green algae during uptake dissolved inorganic carbon. Plant Cell Physiol. *34*, 649–657.

Smith, G. (1978). Evidence for absorption by exchange-coupled Fe 2+-Fe 3+ pairs in the near infra-red spectra of minerals. Phys. Chem. Miner. *3*, 375–383.

Souza-Egipsy, V., Wierzchos, J., Sancho, C., Belmonte, A., and Ascaso, C. (2004). Role of biological soil crust cover in bioweathering and protection of sandstones in a semi-arid landscape (Torrollones de Gabarda, Huesca, Spain). Earth Surf. Process. Landforms *29*, 1651–1661.

Taylor, T.N., Remy, W., Hass, H., and Kerp, H. (1995). Fossil arbuscular mycorrhizae from the early Devonian. Mycologia *87*, 560–573.

Vasile, M., and Vespremeanu-Stroe, A. (2017). Thermal weathering of granite spheroidal boulders in a dry-temperate climate, Northern Dobrogea, Romania. Earth Surf. Pro. Land. *42*, 259–271.

Weber, B., Scherr, C., Bicker, F., Friedl, T., and Buedel, B. (2011). Respiration-induced weathering patterns of two endolithically growing lichens. Geobiology *9*, 34–43.

Wellman, H.W., and Wilson, A.T. (1965). Salt weathering, a neglected geological erosive agent in coastal and arid environments. Nature *205*, 1097–1098.

Wierzchos, J., and Ascaso, C. (1998). Mineralogical transformation of bioweathered granitic biotite, studied by HRTEM: evidence for a new pathway in lichen activity. Clay Clay Miner *46*, 446–452.

Wierzchos, J., DiRuggiero, J., Vítek, P., Artieda, O., Souza-Egipsy, V., Skaloud, P., and Ascaso, C. (2015). Adaptation strategies of endolithic chlorophototrophs to survive the hyperarid and extreme solar radiation environment of the Atacama Desert. Front. Microbiol. *6*, 934.

Wiggering, H. (1987). Weathering of clay minerals in waste dumps of Upper Carboniferous coal-bearing strata, the Ruhr area, West Germany. Appl. Clay Sci. *2*, 353–361.

Włodarczyk, A., Szymańska, A., Skłodowska, A., and Matlakowska, R. (2016). Determination of factors responsible for the bioweathering of copper minerals from organic-rich copper-bearing Kupferschiefer black shale. Chemosphere *148*, 416–425.

Yu, H., and Leadbetter, J.R. (2020). Bacterial chemolithoautotrophy via manganese oxidation. Nature *583*, 453.

Zhao, Q., and Zeng, D.H. (2005). Phosphorus cycling in terrestrial ecosystems and its controlling factors. Acta Phytoecol. Sin. *29*, 153–163.

iScience, Volume *23*

Supplemental Information

Lichens Bite the Dust – A Bioweathering Scenario in the Atacama Desert

Patrick Jung, Karen Baumann, Dina Emrich, Armin Springer, Vincent J.M.N.L. Felde, Stefan Dultz, Christel Baum, Marcus Frank, Burkhard Büdel, and Peter Leinweber

Supplemental Information

Lichens bite the Dust –
A Bio-weathering Scenario in the Atacama Desert

Patrick Jung, Karen Baumann, Dina Emrich, Armin Springer, Vincent J. M. N. L. Felde, Stefan Dultz, Christel Baum, Marcus Frank, Burkhard Büdel, Peter Leinweber

Supplemental Information

Transparent Methods

Site description

Pan de Azúcar National Park is located between 25°53′ to 26°15′S and 70°29′ to 70°40′W along the coast of Chile and is characterized by an arid climate (Lehnert et al., 2018; Baumann et al., 2018). Here, a narrow pediment close to the coast is followed by a steep mountain ridge reaching elevations up to 850 m a.s.l.. After this first mountain ridge, the terrain descends slightly to elevations between 400 and 700 m a.s.l. towards the inland. This study was conducted in 2.5 km distance from the Pacific coast (Lat: 25.96636111°S, Long: 70.61521111°W), where granitoid is the bedrock. The igneous rock granitoid is coarse grained and composed mostly of quartz, alkali-feldspar and plagioclase, whereas micas occur in minor amounts. Slightly altered granitoid rocks are exposed in the upper part of hills (Oeser et al., 2018; Bernhard et al., 2018), which have a conical shape due to weathering and erosion. On the bedrock as well as on rocks/stones of various sizes biocoenoses of lithobiontic communities were observed. On the grit-sized stones (‘grus’), this biocoenosis even caused abundant blackish patterns in the landscape (Fig. 1) thus forming the so-called *grit crust* (Jung et al., 2020; called black grit). The heavily colonized blackish parts could be distinguished from only very little colonized whitish appearing parts (Jung et al., 2020; called white grit).

Sampling procedure

In July 2017, samples were collected from the grit-paved area. For petrographic descriptions, samples of black and white grit were collected. They were taken from three independent 25 x 25 cm plots each by removing the upper centimeter with a broad bristle brush. Similarly, samples for soil texture, element analyses and enzyme

activity analyses were collected from plots of black grit. For soil texture, elemental analyses, the same procedure was applied to the same plots to remove the second centimeter. Samples for geological thin sections, microscopy and X-ray computed microtomography analyses as well as photobiont isolation were taken by pressing five sterile Petri dishes into the ground (black grit). All samples were shipped and stored air-dry until further analyses.

Dust was collected from a plastic sheet (31 cm x 43 cm), which had been carefully attached to the ground by pegs. After 10 days of exposure to the open air, the dust was wiped off with a P-free filter paper, which was slightly wetted by double distilled water (ddH_2O) and placed in a Falcon tube for transport.

Mineralogical analyses of black and white grit samples

For mineralogical analyses, three field replicates of black and white grit (first cm), respectively, were combined. To release contained fine particles in grit stones the samples were finely ground in a ball mill to < 0.5 mm before the clay fraction < 2 µm was separated quantitatively by the Atterberg method by repeated sedimentation (11 times). Electrical conductivity (EC) and pH of the sample fractions were determined in a 1:10 aqueous extract (4.5 g sample and 45 mL deionized H_2O). The EC of deionized H_2O was 0.8 µS cm^{-1}. The concentrations of F^-, Cl^-, NO_2^-, Br^-, NO_3^-, PO_4^{3-}, SO_4^{2-}, Na^+, NH_4^+, K^+, Mg^{2+} and Ca^{2+} in the 1:10 aqueous extracts were quantified with a Metrohm IC instrument (930 Compact IC Flex). The standard solution with the lowest concentration was 0.25 mg L^{-1}. Measured values below this concentration were not evaluated. The validity of the determination of anions and cations was determined by calculating the charge balance ($mmol_c$) of anions and cations. Chemical composition of the two particle size fractions was determined with an XRF analyzer (S1 TITAN, Bruker; Middlesex, USA). The > 2 µm samples were gently ground with a mortar before

analysis of the dry powders. For identification of the clay minerals, the exchange sites of the < 2 µm fraction were saturated with Mg, transferred to glass slides and allowed to dry at room temperature. For the samples, X-ray diffraction patterns were obtained with an X-ray diffractometer (Siemens D500, Germany, Cu Kα radiation). The > 2 µm fractions were ground in a mortar and precipitated to glass slides before X-ray diffraction analyses.

Soil texture and element content of grit stones and dust samples

Soil texture was determined on a combined sample of three field replicates for black grit from the first and second cm, respectively, using sieving and sedimentation procedures after Blume et al. (2010). For elemental analyses, substrates of the first and second cm of three samples were ground to < 0.5 mm using a mixer mill (Retsch MM 200, Haan, Germany) operated at 30 Hz for 5 min with metal beads. Each sample was analyzed in duplicate. Total C, N, and S content was obtained by dry combustion using an elemental analyzer (VARIO EL, Elementar Analysensysteme GmbH, Hanau, Germany). Inorganic C (C_{inorg}) content was determined by Scheibler calcimeter and organic C (C_{org}) content was calculated by subtracting C_{inorg} from total C content (Blume et al., 2011).

For total elemental analysis, 0.5 g dry substrate or the whole filter paper with adhering dust (dust sample), respectively, was extracted using microwave-assisted digestion with aqua regia solution (3:1 hydrochloric acid : nitric acid) (Chen and Ma, 2001; ISO standard 11466). The elemental concentrations were then determined by inductively coupled plasma optical emission spectroscopy (ICP OES) (JY 238 UL Trace, France). Sequential P fractionation was carried out after Hedley et al. (1982), with slight modifications. Solubility of the fractions was assigned to labile P (resin-P and $NaHCO_3$-P), moderately labile P (NaOH-P), relatively stable P (H_2SO_4-P) and non-extractable P

(residual-P). Total P concentration in the fractionation extracts was determined by ICP OES at 214 nm wavelength.

Scanning electron microscope – energy dispersive X-ray analysis (SEM-EDX)

To visualize structures and elemental distributions on single black grit stones, a field emission scanning electron microscope (SEM, MERLIN® VP Compact, Carl Zeiss Microscopy GmbH, Oberkochen, Germany) equipped with an energy dispersive X-ray (EDX) detector (XFlash6/30, Bruker Nano GmbH, Berlin, Germany) was used. Before analysis, the grit-stones were fixed by hot glue on 0.5”SEM Pin Stubs (agar scientific; Plano GmbH, Wetzlar, Germany) and coated with carbon under vacuum (EM SCD 500, Leica Microsystems GmbH, Wetzlar Germany). SEM images were taken at 5kV up to 25 kV and elemental distributions were analyzed using SEM-EDX Quantax Esprit software (version 2.0, Bruker Nano GmbH, Berlin, Germany).

Preparation and microscopy of thin sections and cross sections of lichen thalli

To visualize colonization of the grit stones, thin sections of single black grit stones were prepared. Grit stones including inhabiting organisms (n = 50) were fixed, dehydrated and embedded in acrylic resin (LR-white; London Resin Company, London, UK) according to Bungartz et al. (2004). All steps were conducted in a vacuum chamber. The embedded samples were polished on one side, fixed to glass slides and polished to a thickness of approximately 30 µm. In addition to light microscopy the thin sections were investigated under a fluorescence microscope (Axioskop; HBO 50; Carl Zeiss, Jena, Germany) with 200-fold magnification and AxioVision software (Carl Zeiss, Jena, Germany). The autofluorescence of the green algal photobionts (red) as well as of the fungal hyphae of the lichens (white) was visualized (blue-violet 395-440 nm excitatory 577 filter; 460 nm chromatic beam).

In addition to the thin sections, also cross sections of hydrated lichen thalli were prepared by using lichen thalli, which were detached from black grit stones. They were cut with a cryo-microtome to visualize the inner structure of the thalli. The 20 to 25 µm thin cross sections were transferred with a fine brush to a drop of water on an objective slide, covered with a cover slip and investigated by light microscopy (Axioskop, Carl Zeiss, Jena, Germany) using oil immersion and a 630-fold magnification.

X-ray computed tomography analysis

To investigate the swelling and shrinking potential of single black grit stones during wet-dry cycles, computed microtomography (µCT) scans were done using a Zeiss Xradia 520 versa (Jena, Germany). A single colonized grit stone was first scanned in a dry state, using 80 keV and 1600 projections with an acquisition time of 3 sec. The resulting voxel edge length was 13.41 µm. The projections were then reconstructed as an 8 bit greyscale tiff image stack with 1012 slices. After the first scan, the sample was submerged in tap water for 10 min, to allow the lichen tissue to become fully hydrated. Then, the grit stone was placed in a closed falcon tube and allowed to equilibrate in the dark overnight, in order to prevent the sample from swelling or shrinking during the second scanning process, as this would have resulted in blurred images. The same scanning parameters were used for the second scan of the hydrated grit stone.

Image analysis was done using the software ImageJ (Schindelin et al., 2012). For noise reduction, we used the non-local means denoising algorithm (Buades et al., 2011) with default settings. This filter works like Gaussian blurring, but preserves edges and boundaries. The segmentation was done using the trainable WEKA segmentation plugin for ImageJ (Arganda-Carreras et al., 2017). This plugin is very effective for multiphase segmentation because it combines a collection of machine learning algorithms with a set of selected image features to produce pixel-based segmentation.

Briefly, this plugin can be trained to learn from user input on a training dataset to later perform the same task on an unknown dataset. After manually selecting stone, lichen and pore space, the plugin needed three training runs until it produced a very precise classification of the three phases.

After the segmentation, a median filter with a window size of 2 voxel was used to remove individual isolated voxel from the segmented image. The volume of the different phases was measured by counting the voxels and multiplying them with the voxel resolution. The surface was measured using the “isosurface” algorithm of the BoneJ plugin in ImageJ (Doube et al., 2010). This feature uses marching cubes to create a triangular surface mesh and calculates the object surface as the sum of the areas of the triangles (Lorensen and Cline, 1987). For the visualization of the scans, we used the Vaa3d Software Version 3.2 (Peng et al. 2014), as well as the volume viewer plugin from ImageJ.

Photobiont isolation and culturing

Two single lichen thalli from black grit stones of the first cm were picked manually and crushed in 100 µL ddH_2O before plated on petri dishes with Bold’s Basal Medium (BBM; Bischoff and Bold, 1963) with 1.5 % agarose under sterile conditions. After four weeks two photobiont colonies were picked with a sterile needle under a binocular microscope and plated on fresh BBM plates with 1.5 % agarose. After additional four weeks the plates were checked for pureness and the two pure photobiont colonies were transferred to 200 mL liquid BBM medium as photobiont stocks. Both stock cultures were maintained at 20 µE m^{-2} s^{-1} and a light–dark regime of 16:8 hours at 17 °C. The cultures were shaken several times per day to allow gas exchange with the atmosphere for four months.

Long term pH development of photobionts

To detect the pH development of lichen photobionts, 10 mL of each of the two photobiont stocks were added to 190 mL of liquid BBM media under sterile conditions. Three replicates for each lichen photobiont were prepared in this way and cultivated under the conditions described together with three replicates of 200 mL sterile BBM medium as controls. Every three weeks, 15 mL of each culture and of the controls were decanted into Falcon tubes and the pH was measured with a pH electrode (Meter Lab PHM210, ± 0.01; Radiometer Analytical SAS; Lyon, France). Each replicate was measured three times and a mean value was calculated. The measurements were done in week 0 (starting point of the experiment) and then repeated every three weeks up to 12 weeks.

Short term O_2 and pH development of photobionts

To monitor short term O_2 and pH development of photobionts, experiments were prepared adding 10 mL of each photobiont stock solution to 90 mL of liquid BBM. Three replicates for each photobiont were prepared in this way in glass bottles. During the experiments, which followed Weber et al. (2011), the suspensions were stirred by a magnetic mixer to ensure a gas exchange with the atmosphere in the culture room at 17 °C. Each sample was kept in the dark for 30 minutes for adaptation and pH and O_2 was measured every 2 minutes during an interval of 10 additional minutes in the dark. Oxygen was measured with an O_2 electrode (WTW FDO 925, 0.00-20.00 mg L^{-1} ± 0.5% v. Mw.; Xylem analytics GmbH and Co KG, Weilheim, Germany) and pH with a pH electrode (Meter Lab PHM210; Radiometer Analytical SAS; Lyon, France), which were fixed to the glass bottle to have continuous measurements of both, oxygen and pH. Afterwards the suspensions were exposed to an LED-light panel (PG8 14W LED

Plant Grow Light, Excelvan) as light source to measure pH and O_2 development at different light levels (20, 40, 80, 120, 150, 200, 220 µE). The different light levels were achieved by altering the distance between the light panel and the samples which was controlled with a universal light meter (ULM-500, WALZ, Effeltrich, Germany) that was mounted to the glass bottle. The algal suspensions were allowed to adapt for 10 minutes during exposure of the first light level (20 µE) and pH and O_2 was measured at this light intensity every 2 minutes during additional 10 minutes. Afterwards the samples were exposed to the next light level with a one-minute adaptation period. After the experiments, 1 mL of each algal suspension was taken out and centrifuged. The pellet was re-suspended in 4 mL DMSO and the chlorophyll$_{a+b}$ content was extracted and calculated following Ronen and Galun (1984) as a proxy for the biomass of each culture.

Determination of enzyme activity

From three replicates of each black grit sample (first cm, unground), alkaline phosphatase (ALP), acid phosphatase (ACP), and phosphodiesterase (PDE) activity were determined after Tabatabai and Bremner (1969) and Eivazi and Tabatabai (1977). The enzyme activity was measured in µg p-nitrophenol discharged from a pre-given p-nitrophenylphosphate solution in 1 g material within 1h (µg p-nitrophenol (g h)$^{-1}$).

Statistics

The Shapiro Wilk and Levene's test were used to test the elemental parameters of the first and second cm substrate for normal distribution and homogeneity of variances, respectively. A paired t-test was applied to reveal significant differences between the elemental concentrations of the first and second centimeter. All statistical analyses

were performed using R software version 3.5.3 (R Core team, 2019). Unless otherwise noted, significant differences refer to $P \leq 0.05$.